

# Low level radioactivity assays with HPGe detectors

Xin Ran Liu\*  
Department of Physics and Astronomy,  
University College London,  
Gower Street, London,  
WC1E 6BT

26 August 2013

## Abstract

A low-background high-purity germanium detector located at Boulby underground laboratory has been recommissioned for material screening and selection on behalf of the SuperNEMO neutrinoless double beta decay experiment. In this report, the detector schematic is described in detail along with the calibration process. The detector shielding was also modified to ensure uniform distribution and rigorously cleaned to remove any residual surface contamination. A new radon purging system was installed and operated resulting in a 4 times reduction in the radon levels measured inside the central sample volume as well as improved integrated rate of  $0.751 \pm 0.001$  events/min in the energy range between 100-2700 keV. Further improvements to reduce background are discussed.

---

\*email: x.r.liu@ucl.ac.uk

# Contents

<b>1</b>	<b>Introduction</b>	<b>3</b>
<b>2</b>	<b>Detector Schematic</b>	<b>5</b>
<b>3</b>	<b>Detector Calibration</b>	<b>6</b>
3.1	Energy Calibration . . . . .	6
3.2	Resolution Calibration . . . . .	7
3.3	Efficiency Calibration . . . . .	7
<b>4</b>	<b>Analysis method</b>	<b>9</b>
4.1	Leading industry analysis method . . . . .	11
4.2	Automated analysis . . . . .	12
<b>5</b>	<b>Background Measurements</b>	<b>13</b>
5.1	Shielding improvements . . . . .	13
5.2	Detector relocation . . . . .	15
5.3	Optimising source geometry . . . . .	18
<b>6</b>	<b>Radon effects and measurements</b>	<b>19</b>
6.1	DURRIDGE RAD7 study . . . . .	20
6.2	DURRIDGE RAD7 measurements . . . . .	22
6.2.1	RAD7 Intrinsic Background . . . . .	22
6.2.2	Radon level measurements . . . . .	23
<b>7</b>	<b>Radon Shield Installation and Purging</b>	<b>26</b>
7.1	Nitrogen Flush . . . . .	26
7.2	Radon Shield . . . . .	27
7.3	Diagnostics . . . . .	27
<b>8</b>	<b>Radon Purging Results</b>	<b>28</b>
8.1	Nitrogen flushing at 1 l/min . . . . .	28
8.2	Nitrogen flushing at 5 l/min . . . . .	29
8.3	Improvements to sensitivity . . . . .	30
<b>9</b>	<b>Discussion</b>	<b>31</b>
9.1	Detector improvements . . . . .	31
9.2	Further improvements to radon purging . . . . .	31
9.3	External noise . . . . .	31
9.4	RAD7 . . . . .	32
<b>10</b>	<b>Conclusion</b>	<b>33</b>
<b>11</b>	<b>References</b>	<b>34</b>

# 1 Introduction

Gamma ray spectroscopy using low-level germanium detectors offer a standard method for material screening and selection for rare event searches, such as direct dark matter detection or neutrino mass experiments. The excellent resolution, spectral information and non-destructive measurement makes germanium spectroscopy preferential to other screening methods. Methods such as mass spectrometry which measure only atomic concentrations as well as requiring pre-treatment of sample prior to measurement.

In any naturally occurring material, the main radioactive contaminants are as a result of uranium, thorium and potassium. Other contributors may include cosmogenic  $^{60}\text{Co}$ . For  $^{238}\text{U}$  and  $^{232}\text{Th}$ , the decay chains proceed via either  $\alpha$  or  $\beta^-$  decays as shown in Fig 1.

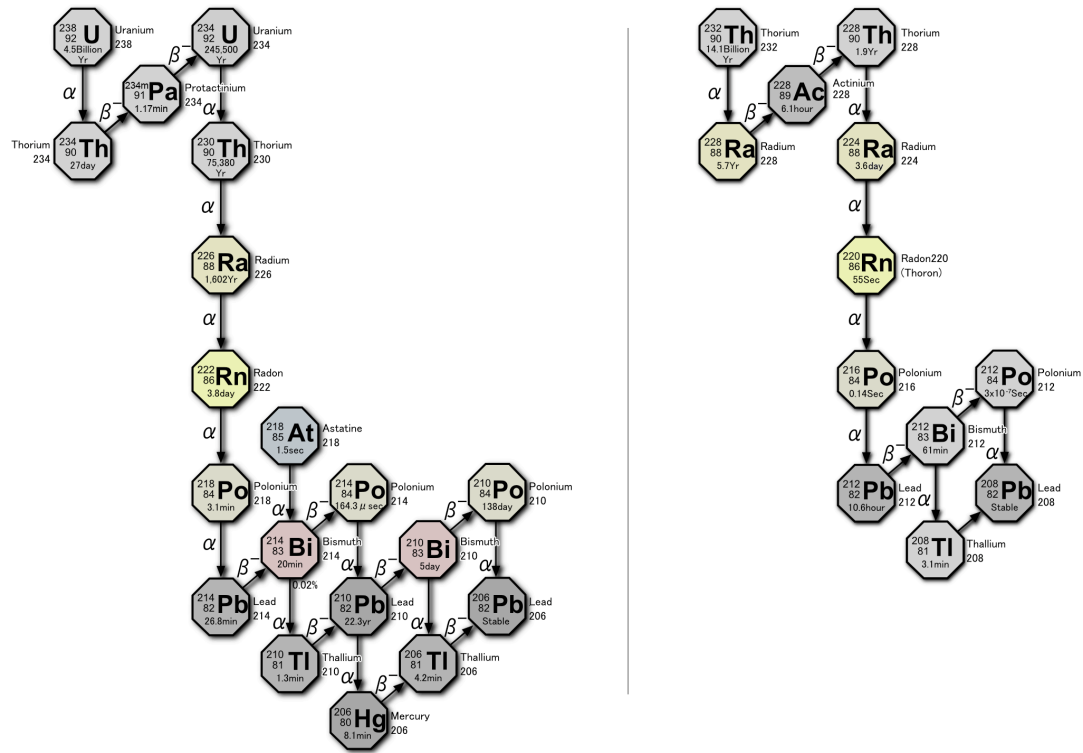


Figure 1: (Left) The decay chain for  $^{238}\text{U}$ . (Right) The decay chain for  $^{232}\text{Th}$ .

A ultra-low background HPGe detector has been recommissioned at Boulby underground laboratory for use in material screening for the neutrino mass experiment SuperNEMO. The laboratory is located 1.1km underground (or 3000 'm w.e.' - metres water equivalent) inside the deepest active mine in Britain. This provides a reduction in cosmic muon flux by six order of magnitude. The decrease in muon flux as well as secondary neutrons are shown in Fig 2.

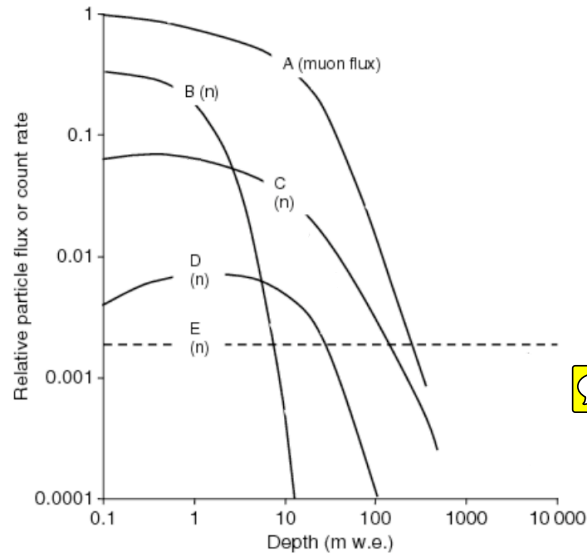


Figure 2: Cosmic muon and neutron fluxes in relation to depth underground. Here A is the cosmic muon flux, B is the secondary neutrons, C is the muon induced neutrons in lead, D is the muon induced neutrons in rock and E is the line showing neutrons from spontaneous fission and  $\alpha, n$  reactions due to uranium and thorium in the rock.

The SuperNEMO experiment is a next generation neutrinoless double beta decay ( $0\nu\beta\beta$ ) experiment. The  $0\nu\beta\beta$  is the most sensitive and perhaps the only practical way to further probe neutrino properties such as;

- absolute neutrino mass;
- if neutrinos are Dirac or Majorana particles;
- neutrino mass hierarchy.

For the double beta decay process to occur, single beta decay has to be highly suppressed energetically. Normal beta decay is energetically forbidden for a nucleus with atomic number  $Z$  if the binding energy of the daughter nucleus (with atomic number  $Z + 1$  for  $\beta^-$  decay) is greater than that of the parent. For double beta decay the daughter nucleus has atomic number  $Z + 2$ , hence for double beta decay to be allowed there must be a suitable nucleus with  $Z + 2$  with a lower binding energy.

Since  $2\nu\beta\beta$  decay requires simultaneous decay of two nucleus, in the same atom, it is an extremely rare event, with a half-life of  $10^{19}$  to  $10^{21}$  years depending on the phase space factor of decay isotope.

The signature of the double beta decay process is the simultaneous emission of two electrons that have energies similar to that of natural radioactivity. Therefore the requirement for radio-pure material is critical.

## 2 Detector Schematic

The detector at Boulby is an Ortec ultra-low background, high-purity, p-type coaxial germanium detector with a sensitive mass of 1.94 kg or a volume of 0.4 litres. The detector is cooled using a cold finger which is in thermal contact with a liquid nitrogen bath. For radio-purity the preamplifier is placed outside the detector shielding as shown in Fig 3.

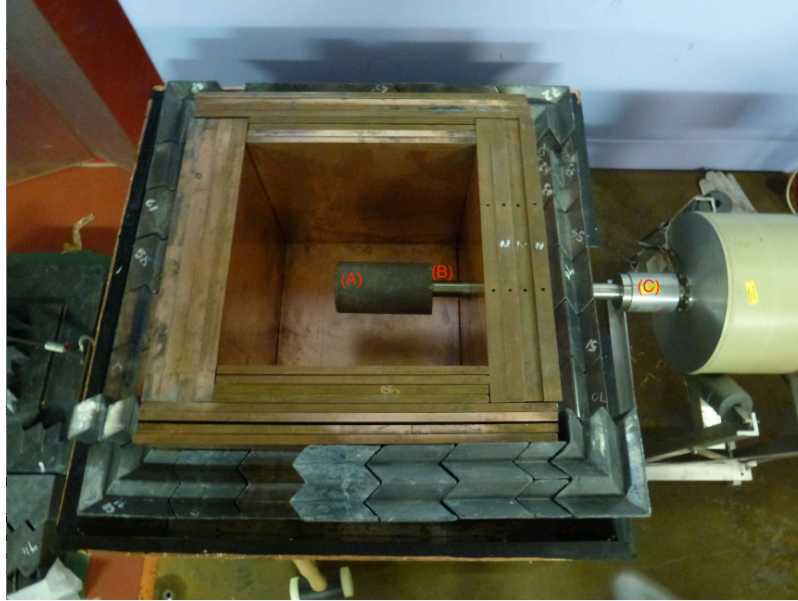



Figure 3: Boulby detector layout with (A) the Mg endcap, (B) the cooling finger and (C) the preamplifier shown.

The detector shielding has been **configure** to allow a large sample capacity of 60 litres (40cm×40cm×40cm). This large volume also minimises backscattering which can cause unwanted features in the measured spectrum. The magnesium endcap is **surround**, from the outside, by 10cm of interlocking lead bricks, which **has** been kept underground for more than twenty years. This is followed by 10cm of high-purity copper which is used to reduce the  $^{210}\text{Pb}$  gammas,  $^{210}\text{Bi}$  bremsstrahlung as well as the fluorescent X-rays from the lead. In order to remove electronic noise, detector and the cryostat was kept electrically isolated from the shielding by inserting insulation around the stem of the detector.

The existing detector shielding was modified to ensure uniform coverage of the detector, no direct line-of-sight to the detector end cap and reproducibility for consistent measurement results. Before reconstruction, the copper was cleaned using diluted acidic solution to remove any residual surface contamination, then wiped down using deionised water. The lead was cleaned using an alkaline solution to also remove surface contamination and then wiped down using isopropyl alcohol before being reassembled. 

### 3 Detector Calibration

There are three main calibrations in order to interpret the gamma-ray spectrum obtained using Gamma-vision in terms of measured activity;

- Energy calibration - to convert from ADC to energy;
- Resolution calibration - to determine the variation of peak width as a function of energy;
- Efficiency calibration - the ratio of counts **observe** to number of decays as a function of energy.

The detector is calibrated regularly with radioactive sources such as  $^{137}\text{Cs}$ ,  $^{60}\text{Co}$ ,  $^{57}\text{Co}$  and a Multi-Gamma source (MGS) containing in addition  $^{65}\text{Zn}$  and  $^{155}\text{Eu}$ . The MGS activity is known and is certified by Canberra to within 5% accuracy.

#### 3.1 Energy Calibration

The data is recorded using a 13 bit ADC which is used with the amplifier and a multichannel analyzer (MCA) to generate **a** spectra consisting of 8192 bins, which can be converted to energy through an energy calibration. This was achieved by taking one hour **spectrums** of known gamma sources, such as  $^{60}\text{Co}$ , which emits 1173 keV and 1332 keV gammas, and recording the peak positions in **ADC**. Several sources were used to ensure the calibration energies cover the entire range over which the spectrometer is to be used. Then a plot of the mean energy peaks in ADC against the true energy can be made as shown in Fig 4.

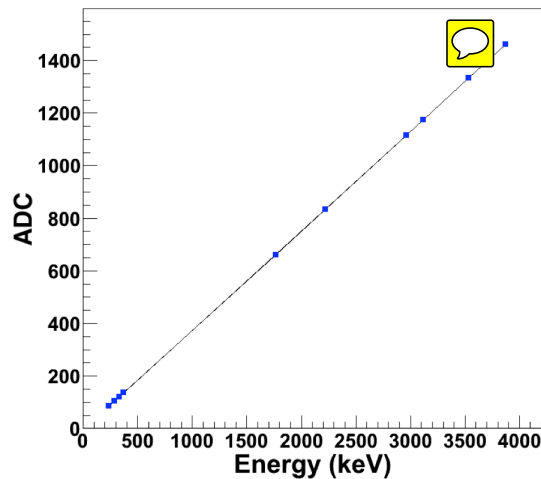


Figure 4: Energy calibration using  $^{137}\text{Cs}$ ,  $^{60}\text{Co}$ ,  $^{57}\text{Co}$  and a MGS fitted to obtain the energy to ADC conversion.

### 3.2 Resolution Calibration



Using the same data set as the energy calibration, a resolution calibration was also performed. This is critical since the data obtained from the detector will be analysed using a computer programme which requires to know how the shape of the peak varies with energy. The energy resolution of the detector is defined as the ratio of the  $\sigma$  to the mean energy of the gamma line as shown in Fig 5.

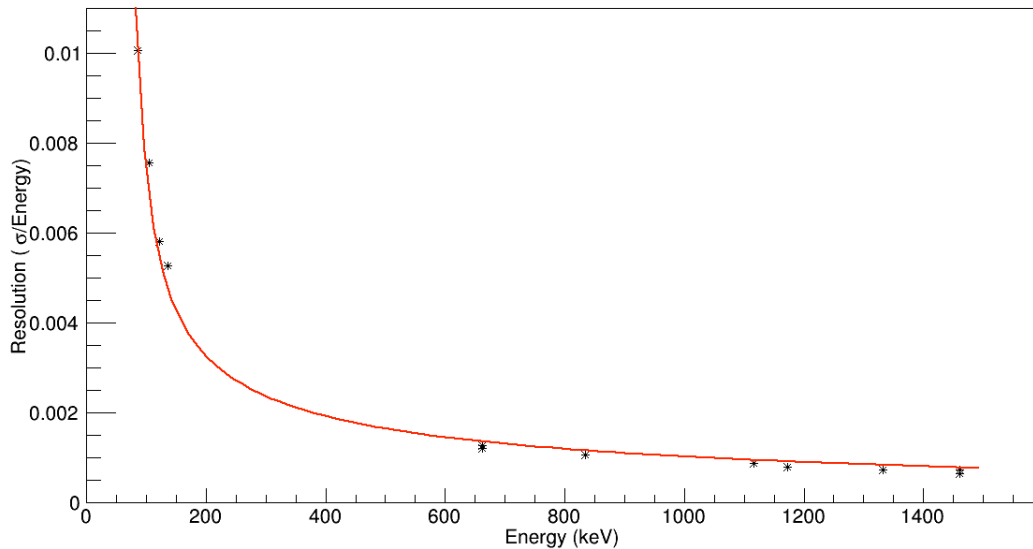


Figure 5: The detector energy resolution plotted here as a function of the mean energy.

### 3.3 Efficiency Calibration

In this case, efficiency refers to the detection efficiency,  $\varepsilon$ , of a particular gamma line which is defined as the ratio between the number of counts detected in a peak to the number of **gamma** of that energy emitted by the source. It is calculated from Monte Carlo (MC) simulations using Geant4[1] by constructing a source with known number of gamma ray emissions and energies then analysing the resultant spectrum. For each material measurement, the MC must be tailor made as it depends on the sample geometry and position on the detector.

The reference data for gamma ray energies, the branching ratio of each decay process and the nuclide half-life used for generating the MC were sourced from the National Nuclear Data Center[2].

To verify the detection efficiency MC, the activities of the MGS was calculated from the one hour calibration measurement and compared with that of the certified values. The shape, position and geometry of the MGS was measured and simulated using Geant4 in

order to get agreement with data. The source is concentrated at a point inside a plastic disk as show in Fig 6.

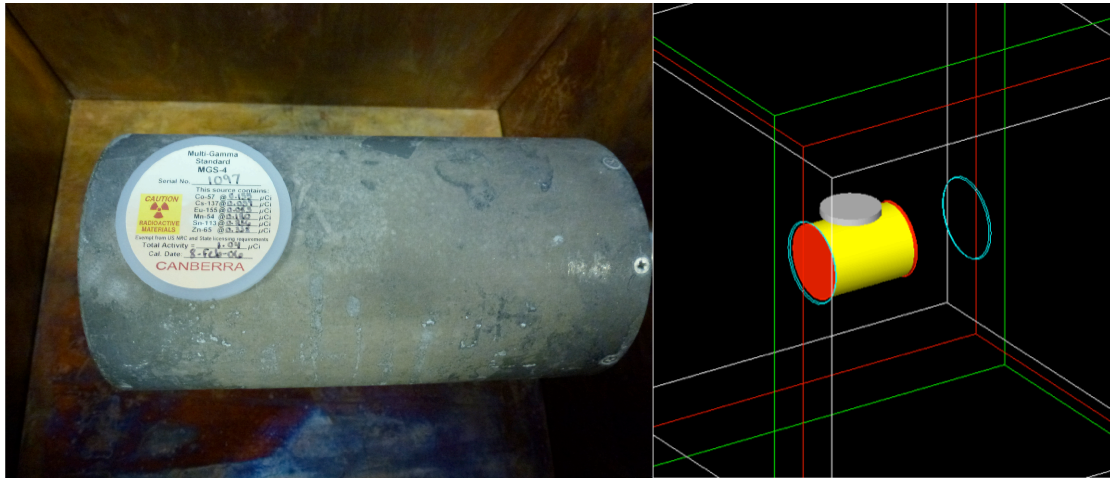


Figure 6: (Left) The MGS on the detector endcap for measurement. (Right) Simulated MGS on detector endcap at the same location in order to determine detection efficiency.

A plot of the MGS spectrum generated using MC is shown in Fig 7 and this is compared with the spectrum of the same source obtained for calibration. Within the associated uncertainties, the two spectrums show good agreement. The results show that the HPGe at Boulby is ready to provide reliable measurement of a given samples activity.

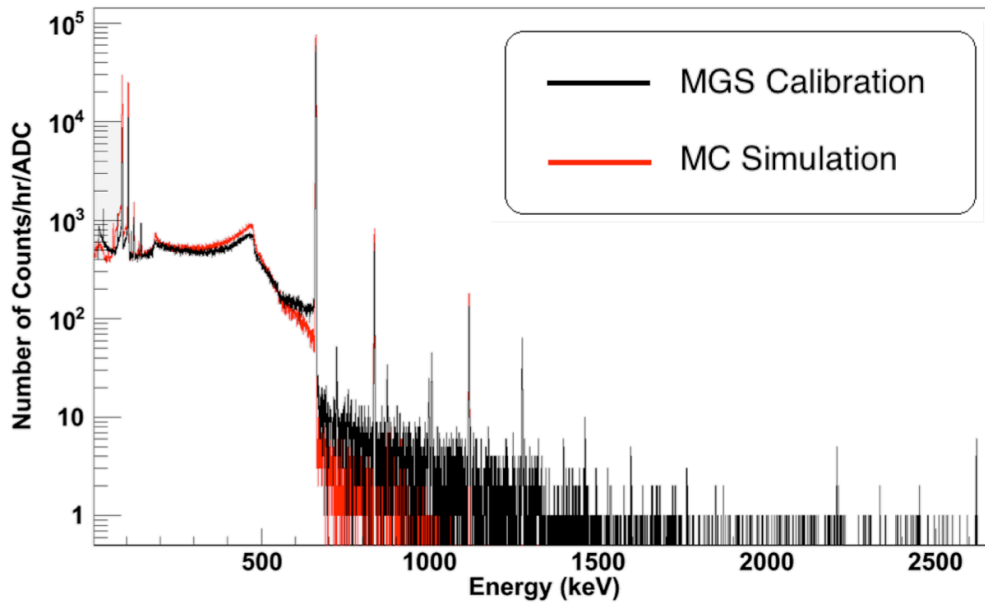


Figure 7: Superposition of two one hour spectrums of a MGS, with the data shown in black and MC in red.



To indicate the detector efficiency, a hypothetical point source placed 5mm above the detector was simulated and shown in Fig 8.

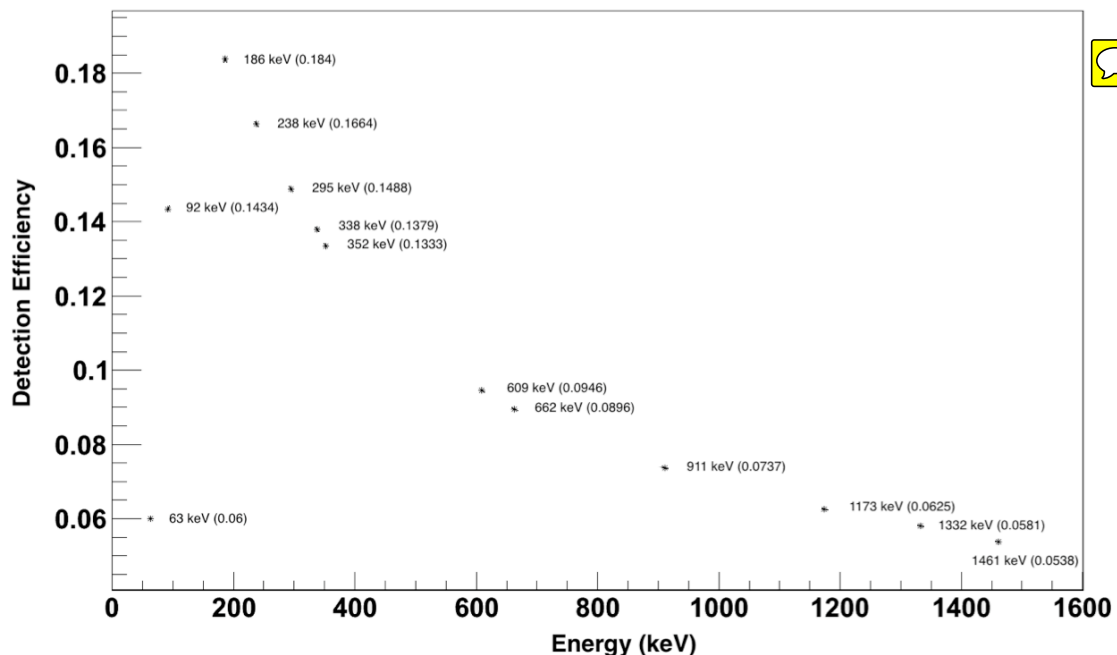


Figure 8: The simulated detector efficiency for a point source placed directly above the detector. The 13 points are the efficiencies at the gamma energies of interest for SuperNEMO material measurements.

## 4 Analysis method

The concentration of radioactive nuclides in a given sample is determined by fitting the  $\gamma$ -lines, using the efficiency as determined by MC simulation taking into account sample geometry and position in the detector.

For the purpose of measurement for SuperNEMO, there are 13 gamma energies of interests are mainly as a result of the  $^{238}\text{U}/^{232}\text{Th}$  decay chains as summarised in Table 1.

The HPGe detector is connected to a PC which has the ORTEC GammaVision-32 software installed. The software takes the signal measured by the detector and produces a spectrum, which is then converted into an energy spectrum following the energy calibration.

The energy **spectrums** are saved as individual 1 hour files over the measurement period. This is due to the daily refill of the detector dewar with liquid nitrogen which results in a significant increase in low energy noise in the measured spectrum. By using 1 hour measurement files, data taken during refill could be isolated and removed.

Decay Isotope	Energy (keV)	Chain/Nuclide	Branching Ratio
$^{238}\text{U}$	63	$^{234}\text{Th} \rightarrow ^{234}\text{Pa}$	0.037
	92	$^{234}\text{Th} \rightarrow ^{234}\text{Pa}$	0.042
	295	$^{214}\text{Pb} \rightarrow ^{214}\text{Bi}$	0.184
	352	$^{214}\text{Pb} \rightarrow ^{214}\text{Bi}$	0.356
	609	$^{214}\text{Bi} \rightarrow ^{214}\text{Po}$	0.455
$^{235}\text{U}$	186	$^{235}\text{U} \rightarrow ^{231}\text{Th}$	0.572
$^{232}\text{Th}$	238	$^{212}\text{Pb} \rightarrow ^{212}\text{Bi}$	0.436
	338	$^{228}\text{Ac} \rightarrow ^{228}\text{Th}$	0.113
	911	$^{228}\text{Ac} \rightarrow ^{228}\text{Th}$	0.258
$^{137}\text{Cs}$	662	$^{137}\text{Cs} \rightarrow ^{137}\text{Ba}$	0.851
$^{60}\text{Co}$	1173	$^{60}\text{Co} \rightarrow ^{60}\text{Ni}$	0.999
	1332	$^{60}\text{Co} \rightarrow ^{60}\text{Ni}$	1
$^{40}\text{K}$	1461	$^{40}\text{K} \rightarrow ^{40}\text{Ar}$	0.107

Table 1: Energies regions of interest for SuperNEMO material screening

A analysis code has been created to open the 1 hour files and remove those with **high low** energy noise. The remaining files are then combined into a single file containing the full spectrum over the measurement period.

The spectrum is then analysed using ROOT[3] and the gamma peaks for each of the 13 energies were **fitted**. The integrated counts in the  $\pm 3\sigma$  energy region was calculated, then using ROOT, the background continuum **can be fitted and subtracted** from the peak areas as shown in Fig 9.

From MC, the detector efficiency at each of the energies can be determined which allow the actual number of gammas emitted at each energy be calculated. Then taking into account the branching ratio, the sample's activity can be determined, this is usually expressed as Bq/kg, by taking into account the sample mass. The equation is as follows;

$$A = \frac{N}{\varepsilon \cdot B \cdot M \cdot t} \quad (1)$$

where A is the sample activity measured as Bq/kg, N is the background subtracted number of counts,  $\varepsilon$  is the detection efficiency, M the sample mass and t the total measurement time in seconds.

The sample activity can be converted to concentrations of radioactive nuclides using the isotope mass (g/mol) and the isotope half-life. The conversion factors used were based on those calculated and published by the UK Dark Matter Collaboration[4].

For  $^{238}\text{U}$ , the gamma-lines from the decay of  $^{214}\text{Pb}$  and  $^{214}\text{Bi}$  were used, assuming **equilibrium**. For  $^{232}\text{Th}$ , the gamma-lines from  $^{228}\text{Ac}$ ,  $^{212}\text{Bi}$  and  $^{208}\text{Tl}$  were used.

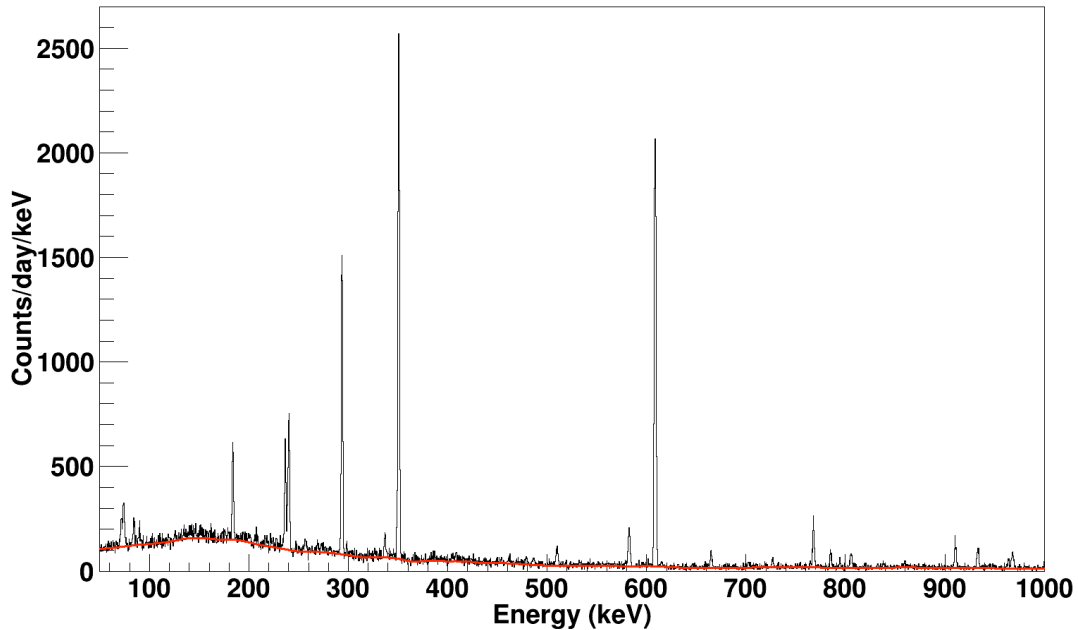


Figure 9: A PMT spectrum is shown to demonstrate the background continuum subtraction applied using ROOT. The spectrum is shown in black and the modelled background continuum is shown in red.


#### 4.1 Leading industry analysis method

The industry leader, Canberra, has developed a software called LabSOCS (Laboratory SOURCEless Calibration Software) in order to determine sample activity and contamination. It is a Monte Carlo based analysis code which also includes a list of fully characterised Canberra detectors which can be selected and incorporated into simulations of detection efficiency. This characterisation is a procedure to determine the detector response to a source being placed within a 500m radius, centred around the detector in free space, over an energy range from 10 keV to 7 MeV[5]. The software also includes a list of sample geometry based on commercially available containers as well as the capability for user defined geometry made of materials which can be selected from a pre-defined library or constructed by user based on chemical composition.

For each sample measurement, the software require only the sample geometry, composition and location with respect to the detector in order to produce an efficiency curve. The software is able then to take a measured spectrum, fit the energy peaks and subtract the background spectrum. Then using taking into account the efficiency curve, produce an value for the activity of the various peaks and convert this to radioactive contamination.

The LabSOCS software is integrated in the Genie 2000 gamma-ray spectrometry sys-

tem of Canberra. This allows the entire process of data capture, detector calibration, efficiency calculation and spectrum analysis to be completed using one software.

This in essence combines the various analysis steps and programmes described in the previous section of this chapter. However, LabSOCS use is limited to characterised detectors only. For characterised detectors, the efficiency calculation does not take into consideration any gamma-ray interaction with material surrounding the detector and sample such as external shielding. Therefore, backgrounds such as Compton scattering are not taken into consideration. 

The efficiency calibration curve generated by LabSOCS also requires the user to enter the associated uncertainties. The manufacturer recommended uncertainties for standard laboratory conditions ranges from 7% at low energies (50-100 keV), 6% at medium energies (100-400 keV) and 4% at high energies (400-7000 keV). These values are significantly higher than what is achievable with standard source based calibrations, hence it cannot yet be used for very high quality measurements.

## 4.2 Automated analysis

Motivated by the near autonomous LabSOCS, the analysis steps and codes described in the first section of this chapter was integrated into one single analysis code. Firstly the noise files are removed, then the detection efficiency must be determined for each measured sample using MC.

Then a file analysis script is called to summed the individual files, plot the energy spectrum and fit the 13 predetermined energy peaks. The background is subtracted with the mean energy and number counts in the  $3\sigma$  region determined. The fitted plots are then written out as a PDF file, with each analysed peak saved in the format shown in Fig 10.

The code then takes the efficiency determined by MC and the branching ratio to give the activity in Bq/kg which is then converted to a uranium, thorium and potassium contamination for each sample.

This closely resembles the LabSOCS system with an efficiency determined using Geant4 which does take into account shielding around the detector and source.

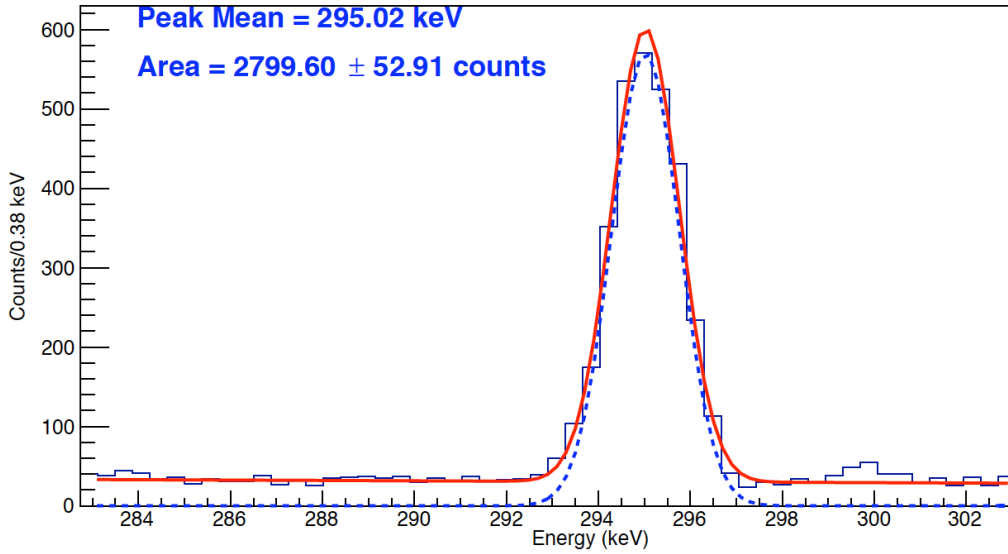


Figure 10: The  $^{214}\text{Pb}$  decay peak at 295 keV. The red and blue line shows the peak fit before and after subtraction of the background continuum.

## 5 Background Measurements

This chapter describes three long background measurement which were made, first to determine if modifications to the detector shielding has made any improvements by lowering the counts in the background spectrum. This was followed by a second background measurement to determine if the background spectrum was stable. The detector was then relocated, resulting in a second cleaning of all the shielding materials as well as a further long background measurement to ensure the detector performance has not deteriorated or alter significantly at the new location.

### 5.1 Shielding improvements

The first measurement to be carried out, after the detector calibrations, was a 1 month background measurement in order to determine if the detector was still fully operational and if so to measure the background levels inside the detector. This is shown in Fig 11, where the main observable energy peaks of interest are labelled.

From this the integrated counts from 100-2700 keV was determined and compared with data taken before the shielding modifications. The result are shown in table 2. This shows a clear improvement of more than 20%. However, when compared against world leading low background detectors such as Gator currently being operated at Gran Sasso background laboratory[6] there are still significant improvements possible.

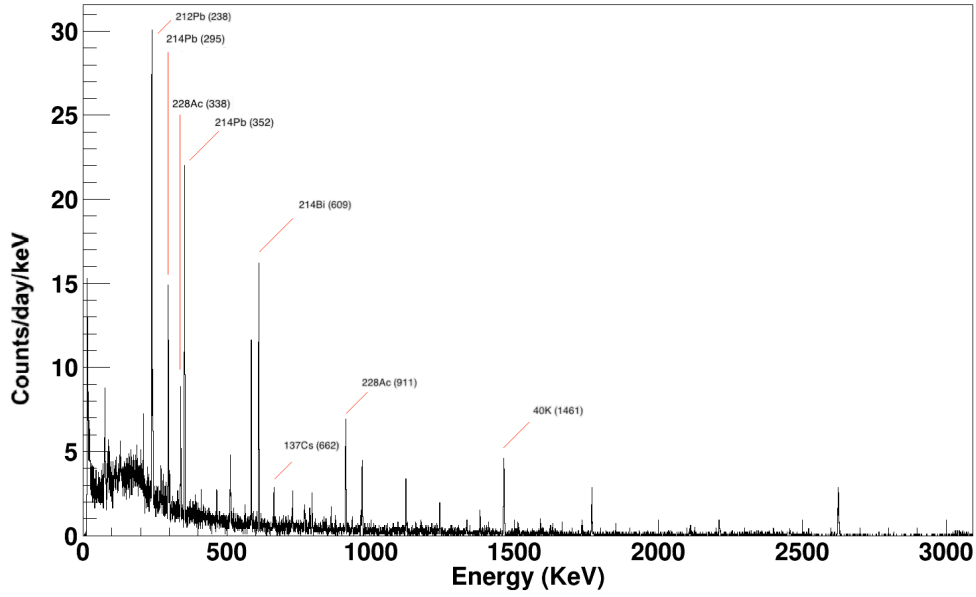


Figure 11: Background spectrum taken over 4 weeks and normalised to counts per day per keV. The labelled peaks are the peaks observed out of the 13 peaks of interest.

Detector Configuration	Events / min
Boulby before shielding modification	$1.303 \pm 0.005$
Boulby after shielding modification	$1.081 \pm 0.003$
The Gator facility (LNGS)	0.16

Table 2: Integrated counts over the range 100-2700 keV, measured as the number of event detected per minute.

A second long background measurement over 4 weeks was conducted in order to compared with the first to determine if the background has remained relatively constant. From analysis of the resultant spectrum, shown in Fig 15, the integrated counts in the energy peaks of interest has remained, within uncertainties, unchanged.

From the background activities, the sensitivity of the detector to the  $^{238}\text{U}$  and  $^{232}\text{Th}$  lines was calculated using the equation;

$$S = \left( \frac{1}{86.4} \right) \cdot \left( \frac{1.64}{Br \cdot \epsilon} \right) \cdot \sqrt{\frac{B}{t}} \quad (2)$$

Where S is sensitivity measured in (mBq/kg) and Br is the isotope branching ratio,  $\epsilon$  is detection efficiency, B is the background counts in the  $\pm 3\sigma$  of the mean energy region

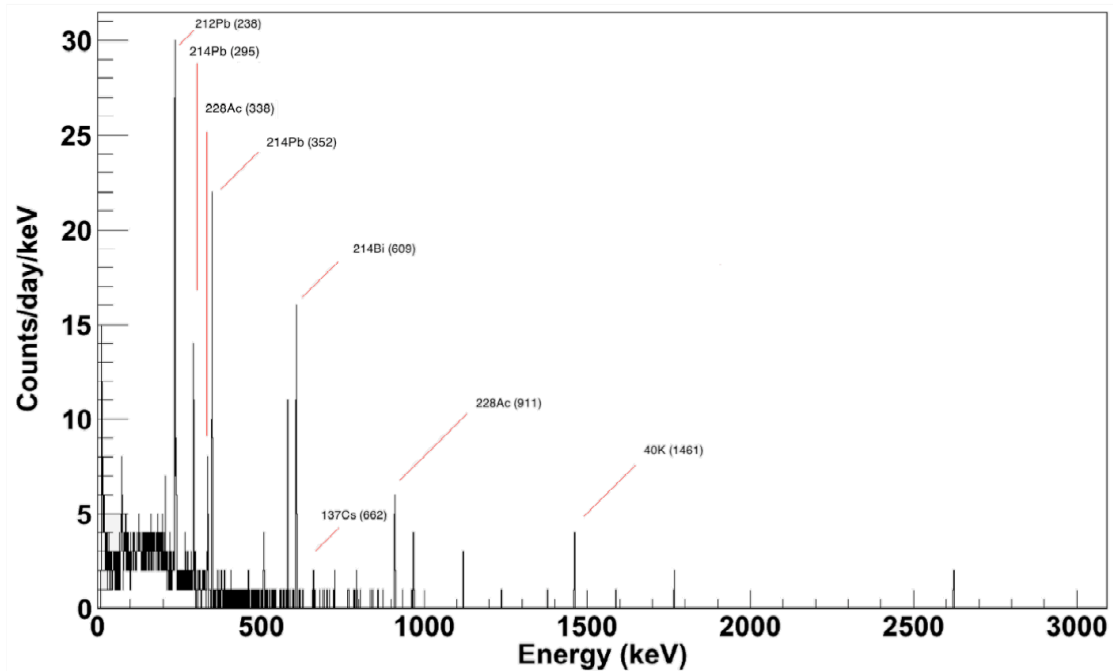



Figure 12: Background spectrum taken over 4 weeks and normalised to counts per day per keV. The labelled peaks are the peaks observed out of the 13 peaks of interest.

and  $t$  is time measured in days. The efficiency used to estimate the sensitivity was taken  half of the point source efficiency simulated in chapter 3, shown in Fig 8.

From the sensitivity equation, the sensitivity as a function of time for  $^{238}\text{U}$  and  $^{232}\text{Th}$  are plotted using the  $^{214}\text{Bi}$  and  $^{212}\text{Pb}$  lines respectively, as shown in Fig 13.

## 5.2 Detector relocation

Before any further measurement could be made, the detector was relocated to a new section of the laboratory. The suitability of the new location was extensively tested before relocation. This was motivated by the observation of disruptions to the detector signal output when the lights are switched on and off in the laboratory.

The same disruption and noise was observed on another germanium detector which observed it more distinctly as it was operating without an preamplifier. Using this detector which was more sensitive to noise, it was found that the noise signal was not only observed when lights were switched on and off, but more persistently at times in the day. Through systematic testing it was established this noise signal was as a result of a flickering fluorescent light bulb more than 50 m away in another area of the laboratory. On replacement of the bulb, the noise was removed. This effect could be reduced by the use of filament bulbs which are less likely to transmit noise to the preamplifier.

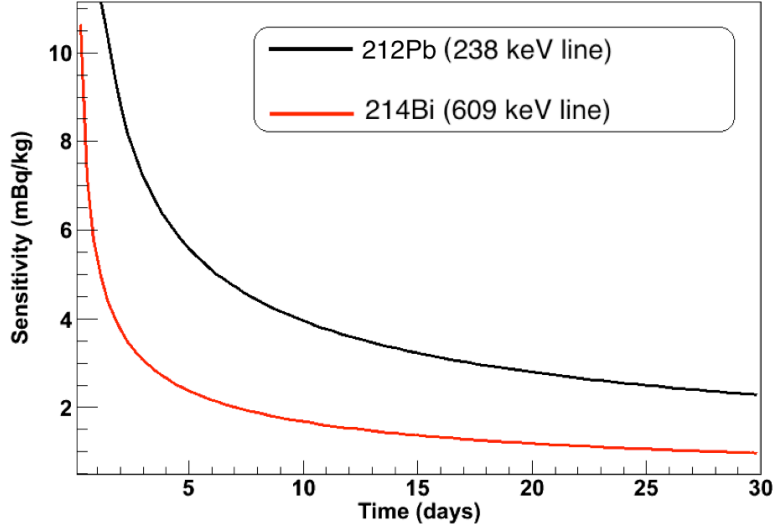


Figure 13: Sensitivity plotted for  $^{238}\text{U}$  and  $^{232}\text{Th}$  using the  $^{214}\text{Bi}$  and  $^{212}\text{Pb}$  lines respectively

The output signal of the detector at the original location was monitored and recorded using an oscilloscope. Then detector was kept cool and moved to the new location where it was reassembled. The new location was also near a cryo generator, which was then switched on and the same procedure was repeated. This data was then analysed to determine if there are any variations in the RMS of the noise signal as seen in Fig 14.

The resultant distributions show little variation between the two locations and also at the new location with the cryo generator switched on. Therefore, the detector and shielding was moved to the new location, cleaned and then reassembled. Additional modification included the insertion of Pb wires to cover the hole on the detector shielding around the stem of the detector in order to further reduce direct line of sight gammas.

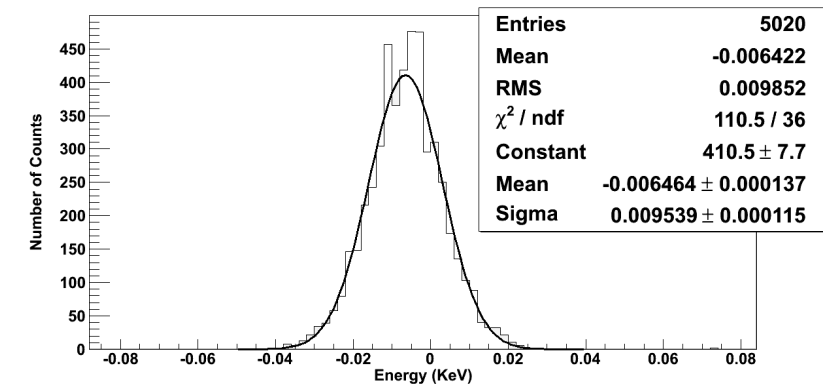
Having replicated the shielding configuration and calibrated the detector, a 2 week background measurement was taken to determine if the detector background has changed. The resultant spectrum is shown in Fig 15. The integrated counts from 100-2700 keV was measured and compared with the previous measurement as shown in table 3.

Detector Configuration	Events / min
Boulby before relocation	$1.081 \pm 0.003$
Boulby after relocation and cleaning	$1.02 \pm 0.01$
The Gator facility (LNGS)	0.16

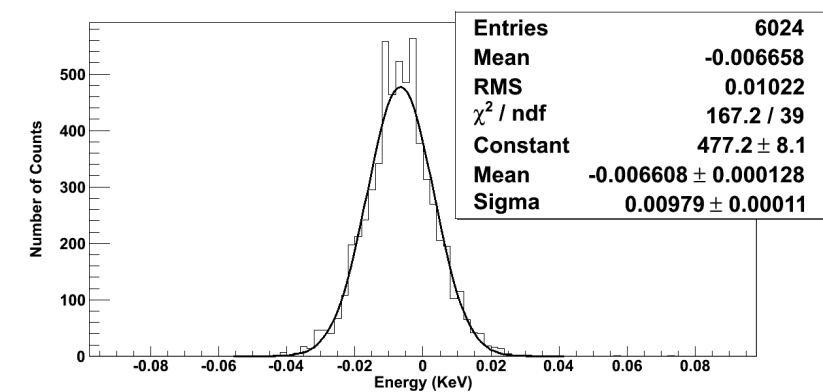
Table 3: Integrated counts over the range 100-2700 keV measured as the number of event detected per minute.

This shows a slight overall reduction in counts detected in the energy region of interest, however there appears to be an increase in  $^{232}\text{Th}$  levels in the new detector configuration.

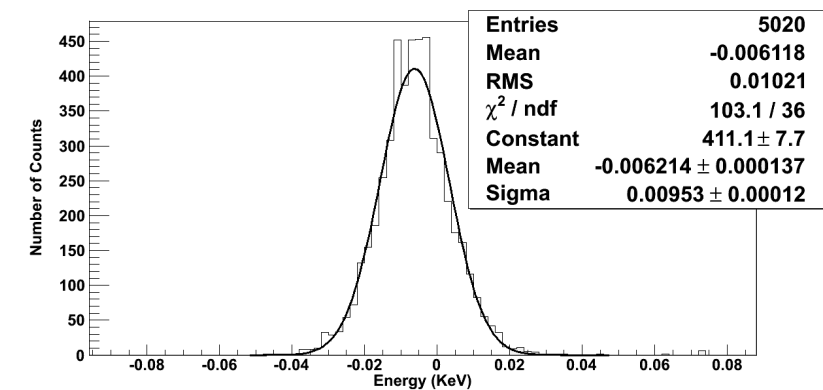




(a) Spectrum taken at the current detector location



(b) Spectrum taken at the new detector location



(c) Spectrum taken at the new detector location with the cryo-generator switched on.

Figure 14: Spectrums comparing the RMS of the signal output from the oscilloscope which was used to record the background noise levels at each of the three locations.

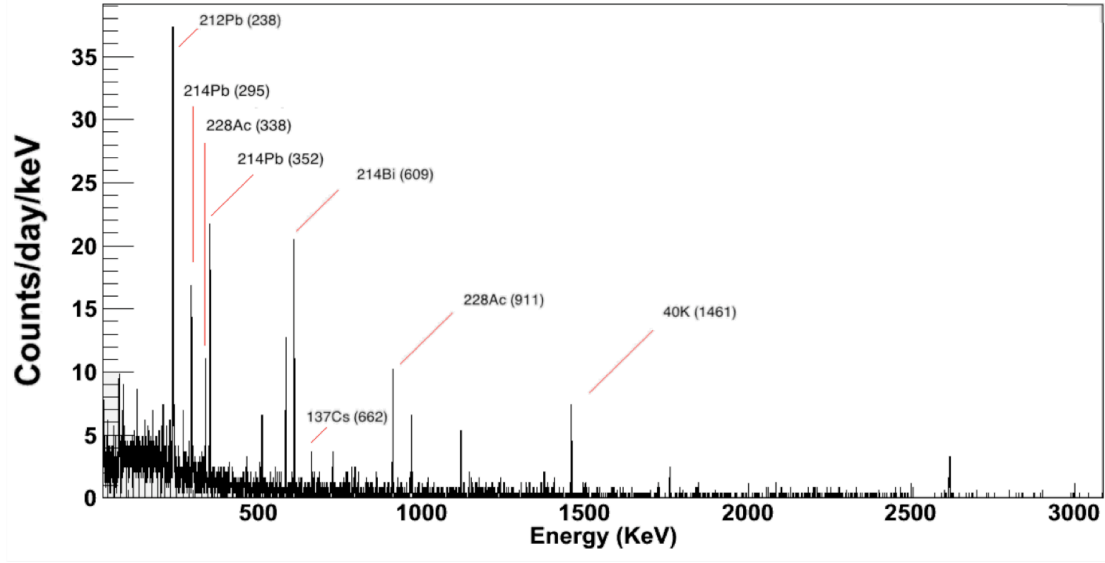


Figure 15: Background spectrum taken at the new location over 2 weeks and normalised to counts per day per keV. The labelled peaks are the peaks observed out of the 13 peaks of interest.

This could be as a result of some contaminants being introduced inside the detector volume prior to the Pb castle being closed.

### 5.3 Optimising source geometry

The detector sensitivity depends on the activity which can be detected after a certain amount of time measured. This depends on the inherent background in the detection volume and the detection efficiency of the sample measured, related by the equation[7];

$$A = \sqrt{b + tB + t^2\sigma_B^2} \cdot \frac{1}{(\varepsilon Mt)} \quad (3)$$

Where A is the activity (Bq/kg), b is the background continuum, t is the measurement time, B is the background counts,  $\sigma_B$  error on the background,  $\varepsilon$  is the detection efficiency and M the sample mass. The activity detected increases with mass until self-absorption of the sample dominates. The detection efficiency of a source can be maximised using MC simulation to determine the optimum sample geometry. Hence each sample can be optimised for measurement.

## 6 Radon effects and measurements

One of the main challenges of all ultra-low background germanium spectroscopy is the presence of radon isotopes in air. This is as a result of emanation from trace amounts of  $^{238}\text{U}$  and  $^{232}\text{Th}$  producing radon,  $^{222}\text{Rn}$ , and thoron,  $^{220}\text{Rn}$ , respectively. Although individually neither has significant gamma-ray emissions, their decay daughter do as summarised in Table 4;

Radon Isotope	Chain/Nuclide	Energy (keV)
$^{222}\text{Rn}$	$^{214}\text{Pb} \rightarrow ^{214}\text{Bi}$	295
	$^{214}\text{Pb} \rightarrow ^{214}\text{Bi}$	352
	$^{214}\text{Bi} \rightarrow ^{214}\text{Po}$	609
$^{220}\text{Rn}$	$^{212}\text{Pb} \rightarrow ^{212}\text{Bi}$	238



Table 4: The daughter nuclides of radon isotopes which emit gamma-rays and the respective energies.

These gamma-lines contribute to the inherent background of the germanium detector, reducing the detector sensitivity. Radon levels inside and around the detector is also variable depending conditions such as temperature, pressure and time of the day, making consistently reproducible background measurements more difficult to achieve.

In order to reduce the effects of radon isotopes inside the detector volume, there are three measures which can be taken;

- make the detector shielding as air-tight as possible to prevent radon diffusion into the detector volume;
- reduce the volume of air inside the detector volume by filling it with sealed containers each filled with radon-free air such as nitrogen or helium;
- flushing the central detector volume with nitrogen to actively remove the radon isotopes. Maintain constant overpressure by continuous flushing to suppress radon diffusion.

All three options would require a reduction in accessibility to the detector. Given the relatively long half-life of  $^{222}\text{Rn}$  and its high diffusibility, it would be difficult to construct a seal sufficiently air tight to prevent diffusion. In particular, there is a path in the current shielding configuration for the stem of the detector to pass through into the central volume. Even if this were possible, there would still be significant contribution of radon as a result of emanation from the Pb and Cu. Even  $^{220}\text{Rn}$  which has a relatively short half-life of just 55 seconds, can still diffused through the outer shielding into the central volume before decaying into daughter isotopes.

Placing sealed containers to displace the air inside the detector has been shown to result in significant reduction in radon contributions to background measurements. However

this requires containers to have very low radon emanation itself as well as a **method fill** and seal them to a satisfactory quality.


Continuous flushing offers the most practical solution to reducing radon isotopes inside the central volume. Indeed many ultra-low background HPGe detector set up includes active purging using either cylindered or boil off nitrogen as a method to reduce radon in the background.

In practice, all three measures should be undertaken to maximise radon reduction. This will be discussed further in the next Chapters.

## 6.1 DURRIDGE RAD7 study

The RAD7 made by 'DurrIDGE Radon Instrumentation' is a portable, fast and highly sensitive radon detector. The inside consists of a 0.7 litre spherical detection volume which has an electrical conductor coated on the inside surface. The center of the volume consists of a solid-state, ion-implanted, planar, silicon alpha detector [8]. A potential ranging from 2000-2500V is created between the conductor and the detector by the application of a high voltage. This generates an electric field throughout the detection volume which accelerates charged particles toward the detector.

The RAD7 detector does not measure **222Rn** directly, instead it measures the daughter isotopes  $^{218}\text{Po}$ ,  $^{214}\text{Po}$  and  $^{210}\text{Po}$ . The  $^{218}\text{Po}$ , which is positively charged, is plated onto the detector as a result of the electric field. It also detects the  $^{220}\text{Rn}$  daughter isotopes  $^{216}\text{Po}$  and  $^{212}\text{Po}$  for thoron measurements. The data is recorded and can be analysed using the software CAPTURE [9].

Other than the number of polonium counts detected, the RAD7 device also records the temperature and humidity of the air it measures. Due to the requirement for  $^{218}\text{Po}$  to drift towards the detector, humidity inside the measurement volume will have an effect on the detection efficiency. This is as a result of the water molecules neutralising the  $^{218}\text{Po}$  atom, hence preventing it from reaching the detector. 

In order to minimise this effect, the air is filtered through a column filled with desiccant which reduces the humidity in the air to 6% assuming operation at room temperature. The experimental setup is shown in Fig 16. The CAPTURE software is also able to perform an automatic correction of the data depending on the humidity levels.

A separate analysis code was written in order **to analysed** the RAD7 data using ROOT independently. This is in part due to the lack of clarity as to the statistical methods applied by the CAPTURE software in processing the data.

In order to understand the humidity corrections used by the RAD7 as well as the detection efficiency of  $^{218}\text{Po}$  and  $^{214}\text{Po}$ , a detailed study was conducted on the CAPTURE software and how it analysed the data taken by the RAD7.

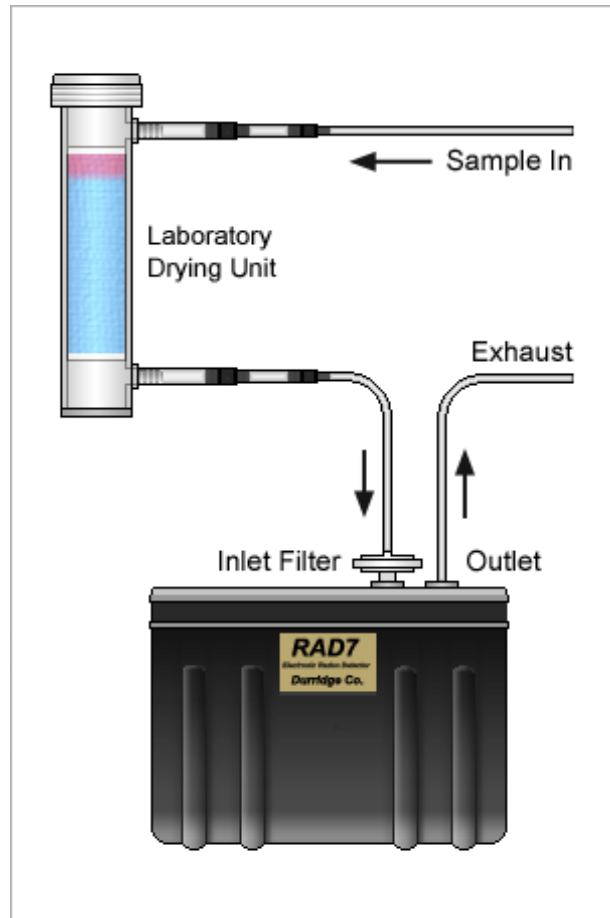


Figure 16: RAD7 standard setup up with the desiccant column attached to the detector inlet.

The RAD7 records the number of counts for  $^{218}\text{Po}$  and  $^{214}\text{Po}$ . However, during the first three hours of operation, only the activity of  $^{218}\text{Po}$  is used for determining  $^{222}\text{Rn}$  levels. This allows for the calculation of the intrinsic efficiency of the detector to  $^{218}\text{Po}$  as determined and used by DURRIDGE. By comparing the radon activity as given by CAPTURE and from calculation based on the number of detected  $^{218}\text{Po}$  decays, a detection efficiency of 23.6% was determined.

After the initial 3 hour period, both  $^{218}\text{Po}$  and  $^{214}\text{Po}$  are used to determine radon activities. The CAPTURE software now uses a combined efficiency of 49.4%, instead of 50% as quoted in the manual, with equal weighting given to both isotopes. Therefore, detection of either a  $^{218}\text{Po}$  or a  $^{214}\text{Po}$  decay is considered as a  $^{222}\text{Rn}$  decay. For long measurements, this could result in double counting of the polonium isotope leading to an over estimation of radon activity.

The method applied by the CAPTURE software to correct for high humidity was determined by first calculating the humidity correction factor used from the raw data. Then

plotting it as a function of humidity as shown in **Fig ??**. This translates to a linear correction function;

$$H_c = (0.0073 \times H) + 1 \quad (4)$$

Where H is the humidity level and  $H_c$  is the humidity correction factor which needs to be applied to the measured radon level.

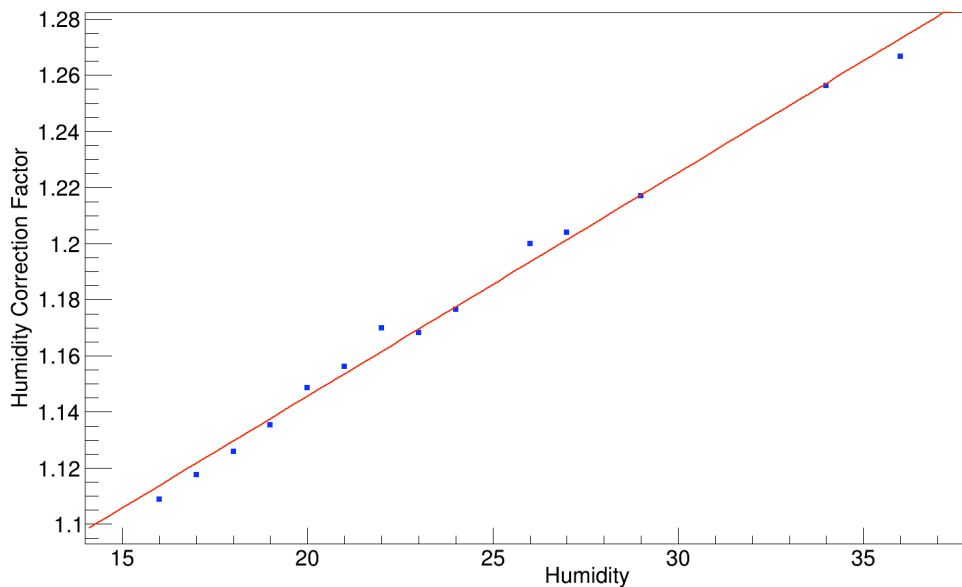


Figure 17: The humidity correction factor applied by the CAPTURE software as a function of measured humidity.

## 6.2 DURRIDGE RAD7 measurements

Having incorporated the humidity correction factors and the detection efficiencies into the analysis code, measurements were made to study the intrinsic background of the RAD7, and then radon levels inside the underground laboratory.

### 6.2.1 RAD7 Intrinsic Background

The RAD7 was placed inside a sealed air tight stainless steel container which was flushed using cylindered nitrogen in order to determine its absolute sensitivity. The nitrogen was flushed at a rate of 5 l/min through the inlet on the side of the container, the

overpressure force air through the outlet, at the opposite corner, which was connected to a long,  $\sim 10$  m, clear plastic tubing leading out of the room. A fan was installed on the inside of container to ensure uniform distribution of nitrogen.

The RAD7 was operated without the desiccant column as the humidity levels of cylinder nitrogen is extremely low. Measurement was made over an 18 hour period and the resultant radon levels are shown in Fig 18. The container was continuously flushed for the first 13 hours, the stopped. During flushing, the humidity clearly falls until it reaches a minimum after 8 hours. When the flushing is stopped after 13 hours, the humidity starts to rise until the experiment is stopped after 18 hours. The detected radon level demonstrates an intrinsic background of  $0.1 \text{ Bq/m}^3$  for the RAD7 detector.

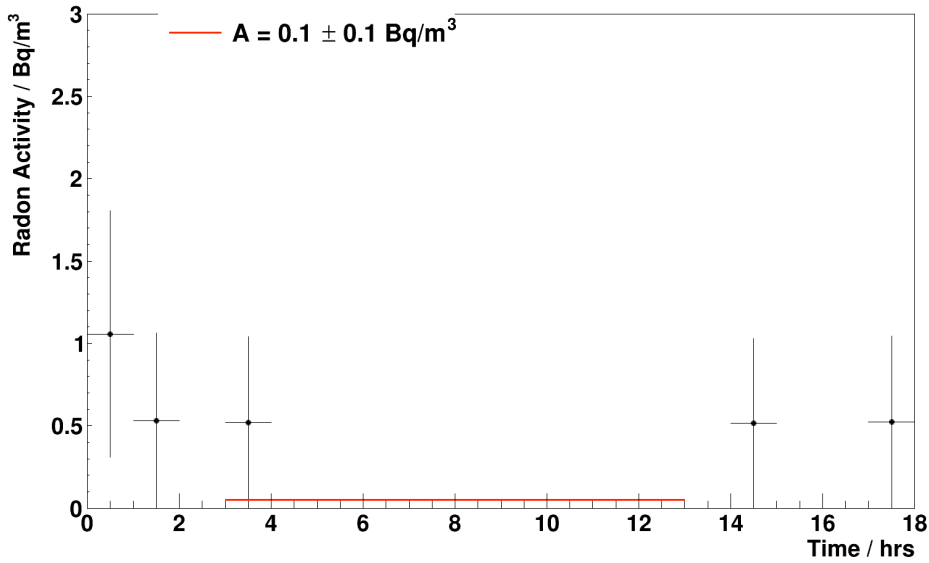


Figure 18: RAD7 background measurement, operating without the desiccant column, over 18 hours.

### 6.2.2 Radon level measurements

Having measured the intrinsic background of the RAD7 and tested the analysis code. The detector was brought underground to monitor and measure the radon levels inside the underground laboratory, in particular the areas around the germanium detector.

The RAD7 was setup with the desiccant drying column and placed on a table top next to the HPGe detector. A 2 day background measurement was taken and the result shown in Fig 19. There appears to be a spike in radon levels in the morning from 6 am to 11 am with unknown origin. However analysing the data before and after the spike separately, the results are relatively consistent and agree with each other within uncertainties.

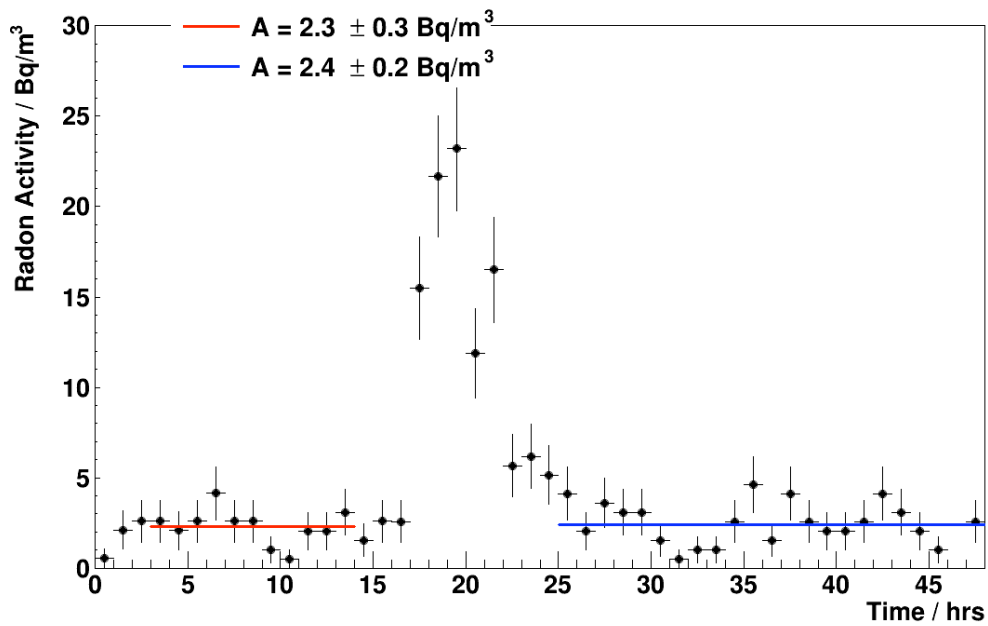


Figure 19: RAD7 measurement with the standard setup up over 2 days.

Following this measurement, a second measurement was made over a 10 day period giving much greater statistics. The resultant plot is shown in Fig 20, and the radon level appear to be much more stable for the duration of measurement.

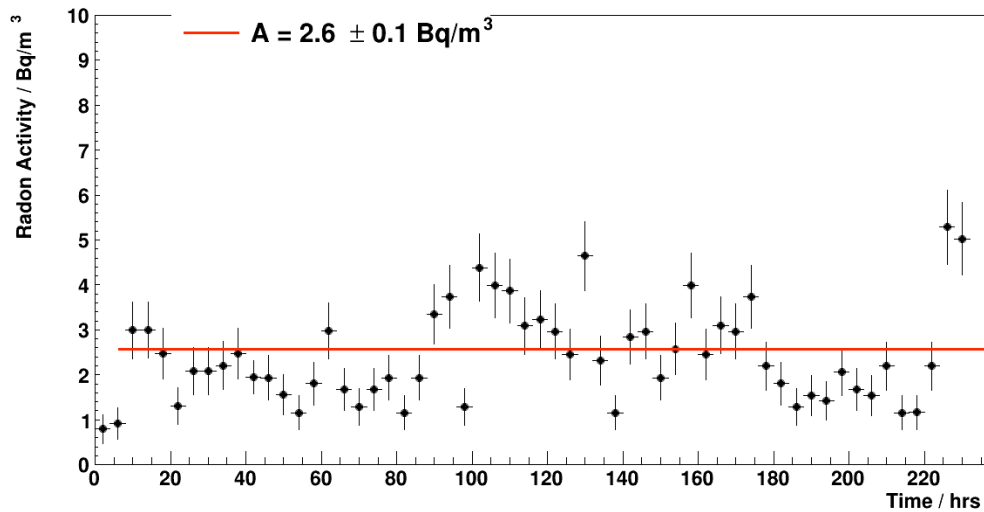


Figure 20: RAD7 measurement with the standard setup up over 10 days.



Combining the three data sets, taking into account the associated uncertainties, gives a radon level of  $2.5 \pm 0.1$  Bq/m<sup>3</sup> inside the laboratory.

However, the desiccant has been shown to itself emanate radon. Hence a DRYSTIK ADS-2[10] was purchased to replace the use of the desiccant column as shown in Fig 21. The DRYSTIK contains two tubes, one inside the other. The inner tube is made of a material called Nafion which is used as a humidity exchanger, permitting the movement of water molecules whilst blocking radon and air. The outer tube is filled with the less humid air from the RAD7 outlet, whilst the air from the inner tube is actively pumped into the RAD7 inlet. This should reduce the air pumped into the RAD7 even further and may give a more reliable radon measurement.

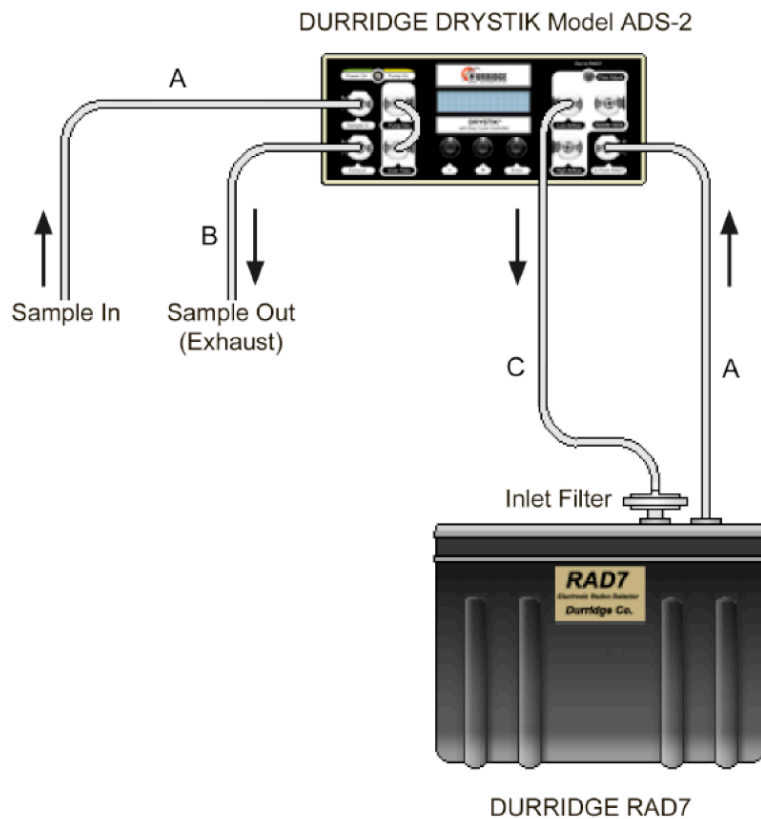


Figure 21: RAD7 setup up with the DRYSTIK-ADS2 replacing the desiccant column. The filtered air is pumped by the DRYSTIK into the RAD7 inlet and the exhaust flows through the DRYSTIK before exiting.

## 7 Radon Shield Installation and Purging

From the measurement of radon **in** levels in the air around and inside the detector, an estimate can be made of the contribution this has to the background spectrum. Since the volume inside the shielding is known, 64 litres, as is the volume of the detector endcap, 1 litres, the amount of radon decays can be estimated. Using Geant4, by confining the radon to the air surrounding the detector, the  $^{222}\text{Rn}$  contribution to the background can be simulated. This is summarised in Table 5 which shows the integrated counts in the  $\pm 3\sigma$  region of the energy peaks of interest.

Chain/Nuclide	Energy (keV)	Boulby HPGe ( $\pm 3\sigma$ )	$^{222}\text{Rn}$ (2.5 Bq/m <sup>3</sup> $\pm 3\sigma$ )
$^{234}\text{Th} \rightarrow ^{234}\text{Pa}$	63	16.7 $\pm$ 1.6	3.85 $\pm$ 0.11
$^{234}\text{Th} \rightarrow ^{234}\text{Pa}$	92	18.8 $\pm$ 1.7	4.41 $\pm$ 0.12
$^{214}\text{Pb} \rightarrow ^{214}\text{Bi}$	295	31.3 $\pm$ 2.2	27.50 $\pm$ 0.29
$^{214}\text{Pb} \rightarrow ^{214}\text{Bi}$	352	39.9 $\pm$ 2.5	46.00 $\pm$ 0.38
$^{214}\text{Bi} \rightarrow ^{214}\text{Po}$	609	34.4 $\pm$ 2.3	38.54 $\pm$ 0.35
$^{235}\text{U} \rightarrow ^{231}\text{Th}$	186	21.3 $\pm$ 1.8	7.60 $\pm$ 0.15
$^{212}\text{Pb} \rightarrow ^{212}\text{Bi}$	238	84.9 $\pm$ 3.7	5.32 $\pm$ 0.13
$^{228}\text{Ac} \rightarrow ^{228}\text{Th}$	338	22.7 $\pm$ 1.9	2.24 $\pm$ 0.08
$^{228}\text{Ac} \rightarrow ^{228}\text{Th}$	911	21.8 $\pm$ 1.9	0.72 $\pm$ 0.05
$^{137}\text{Cs} \rightarrow ^{137}\text{Ba}$	662	6.8 $\pm$ 1.0	1.02 $\pm$ 0.06
$^{60}\text{Co} \rightarrow ^{60}\text{Ni}$	1173	0.5 $\pm$ 0.3	0.39 $\pm$ 0.04
$^{60}\text{Co} \rightarrow ^{60}\text{Ni}$	1332	1.7 $\pm$ 0.5	0.30 $\pm$ 0.03
$^{40}\text{K} \rightarrow ^{40}\text{Ar}$	1461	17.2 $\pm$ 1.6	0.30 $\pm$ 0.3

Table 5: Shows the simulated contribution of  $^{222}\text{Rn}$  in the  $\pm 3\sigma$  regions of the energy peaks of interest for SuperNEMO material screening.

The simulation suggests almost all counts in the 295, 352 and 609 keV energy regions could be removed by removing the radon inside the detector central volume.

### 7.1 Nitrogen Flush

Firstly, a clear PVC pipe was inserted through the detector shielding into the central volume. The pipe was secured on top of the magnesium endcap pointing upwards. This was to prevent the nitrogen from leaking out of the bottom of the detector/shield instead of filling the whole volume.

Cylindered nitrogen was used as the flushing gas as it has extremely low levels of radon. A rack of 15 nitrogen cylinders was connected to the input pipe with a **needle valve** attached to the regular followed by a variable area flow meter to monitor the nitrogen flow rate.

## 7.2 Radon Shield

Having setup the nitrogen flushing system, a shield was constructed on the outside of the current Pb castle to prevent diffusion of radon into the central volume. This was constructed using aluminium and was made in three sections with rubber lining the joints to prevent leakages. The three sections are stacked one on top of the other with three separate joints. The edges were covered using tape to further prevent leakages.

The bottom joint was held in place by gravity whilst the other two were sealed tightly using clamps on the corners and the middle of each side as shown in Fig 22. The gap **were** the stem of the detector passes into the shielding was again sealed using tape to remove any openings for radon to enter. This configuration was used to maximise accessibility whilst providing a air tight seal. Only the lid need to be removed and resealed for each sample measurement.



Figure 22: The radon tent fully constructed and clamped down around the detector with the cylindered nitrogen rack on the right.

A exhaust was made on the mid-section of the radon shield to allow gas exit. A glove was tightened around the outlet to monitor the pressure inside the shield.

## 7.3 Diagnostics

Once the radon shield was fully sealed, the effectiveness of the shield and the nitrogen flushing system was tested by flushing at a very high rate, 30 l/min, to check for any leakages and overpressure. The glove showed clear signs of expansion suggesting an overpressure has been created inside the radon shield. The nitrogen also appears to be flowing freely with no obstruction and minimal leakages.

## 8 Radon Purging Results

Before each measurement with the nitrogen purging system, the central volume was flushed at a high flow rate, 10 l/min, for 60 minutes in order to remove any radon present. Then flow rate was reduced to and maintained at a continuous, predetermined rate.

### 8.1 Nitrogen flushing at 1 l/min

Firstly, a background measurement was taken over 2 week with the nitrogen flushing set at 1 l/min. This rate was chosen as it is used by the LSM germanium facility for radon purging. A comparison of the resultant spectrum with the pre-flushing background spectrum is shown in Fig 23. This shows a reduction in the radon daughter decay peaks by a factor of 4, Table 6.

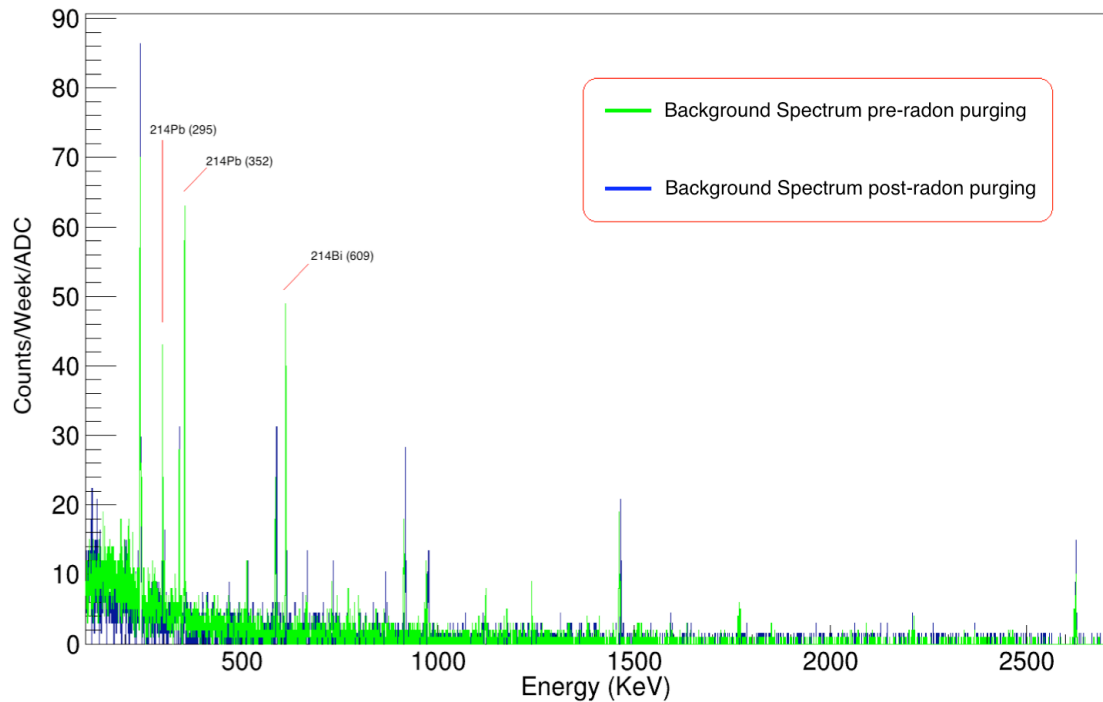


Figure 23: Two superimposed background **spectrums** taken before and after radon purging shown in green and blue respectively. The three labelled peaks are as a result of radon decay isotopes.

The integrated rate between 100-2700 keV was measured to be  $0.751 \pm 0.001$ , a reduction on the pre-radon purging rate by more than 30%. The results also shows a slight reduction in the 238 keV energy peak, more than expected from purging purely radon. This could be as a result of thoron reduction inside the main detector volume, which could explain why only the 238 keV peak was reduced and not the 338 and 911 keV peaks.

Chain/Nuclide	Energy (keV)	Boulby HPGe ( $\pm 3\sigma$ )	Simulated $^{222}\text{Rn}$ ( $2.5 \text{ Bq/m}^3 \pm 3\sigma$ )	Boulby HPGe with radon purging ( $\pm 3\sigma$ )
$^{234}\text{Th} \rightarrow ^{234}\text{Pa}$	63	$16.7 \pm 1.6$	$3.85 \pm 0.11$	$10.3 \pm 0.9$
$^{234}\text{Th} \rightarrow ^{234}\text{Pa}$	92	$18.8 \pm 1.7$	$4.41 \pm 0.12$	$13.9 \pm 1.1$
$^{214}\text{Pb} \rightarrow ^{214}\text{Bi}$	295	$31.3 \pm 2.2$	$27.50 \pm 0.29$	$9.0 \pm 0.9$
$^{214}\text{Pb} \rightarrow ^{214}\text{Bi}$	352	$39.9 \pm 2.5$	$46.00 \pm 0.38$	$9.8 \pm 0.9$
$^{214}\text{Bi} \rightarrow ^{214}\text{Po}$	609	$34.4 \pm 2.3$	$38.54 \pm 0.35$	$8.2 \pm 0.8$
$^{235}\text{U} \rightarrow ^{231}\text{Th}$	186	$21.3 \pm 1.8$	$7.60 \pm 0.15$	$14.4 \pm 1.1$
$^{212}\text{Pb} \rightarrow ^{212}\text{Bi}$	238	$84.9 \pm 3.7$	$5.32 \pm 0.13$	$71.3 \pm 2.4$
$^{228}\text{Ac} \rightarrow ^{228}\text{Th}$	338	$22.7 \pm 1.9$	$2.24 \pm 0.08$	$22.2 \pm 1.4$
$^{228}\text{Ac} \rightarrow ^{228}\text{Th}$	911	$21.8 \pm 1.9$	$0.72 \pm 0.05$	$18.8 \pm 1.3$
$^{137}\text{Cs} \rightarrow ^{137}\text{Ba}$	662	$6.8 \pm 1.0$	$1.02 \pm 0.06$	$6.6 \pm 0.7$
$^{60}\text{Co} \rightarrow ^{60}\text{Ni}$	1173	$0.5 \pm 0.3$	$0.39 \pm 0.04$	$1.7 \pm 0.4$
$^{60}\text{Co} \rightarrow ^{60}\text{Ni}$	1332	$1.7 \pm 0.5$	$0.30 \pm 0.03$	$1.4 \pm 0.3$
$^{40}\text{K} \rightarrow ^{40}\text{Ar}$	1461	$17.2 \pm 1.6$	$0.30 \pm 0.3$	$15.1 \pm 1.1$

Table 6: Comparison of results taken before and after nitrogen flushing at 1 l/min. The area in grey are the radon daughter isotopes decays.

## 8.2 Nitrogen flushing at 5 l/min

The flow rate was then increased to 5 l/min, in order to test if further reduction could be achieved. A new flow meter, by Key Instruments, was installed to monitor the flow rate. The results after a one week measurement are shown in Table 7.

Chain/Nuclide	Energy (keV)	Boulby HPGe ( $\pm 3\sigma$ )	Boulby HPGe with radon purging ( $\pm 3\sigma$ ) 2 weeks at 1 l/min	Boulby HPGe with radon purging ( $\pm 3\sigma$ ) 1 week at 5 l/min
$^{234}\text{Th} \rightarrow ^{234}\text{Pa}$	63	$16.7 \pm 1.6$	$10.3 \pm 0.9$	$12.0 \pm 1.3$
$^{234}\text{Th} \rightarrow ^{234}\text{Pa}$	92	$18.8 \pm 1.7$	$13.9 \pm 1.1$	$19.5 \pm 1.6$
$^{214}\text{Pb} \rightarrow ^{214}\text{Bi}$	295	$31.3 \pm 2.2$	$9.0 \pm 0.9$	$8.0 \pm 1.1$
$^{214}\text{Pb} \rightarrow ^{214}\text{Bi}$	352	$39.9 \pm 2.5$	$9.8 \pm 0.9$	$8.3 \pm 1.1$
$^{214}\text{Bi} \rightarrow ^{214}\text{Po}$	609	$34.4 \pm 2.3$	$8.2 \pm 0.8$	$5.5 \pm 0.9$
$^{235}\text{U} \rightarrow ^{231}\text{Th}$	186	$21.3 \pm 1.8$	$14.4 \pm 1.1$	$13.4 \pm 1.4$
$^{212}\text{Pb} \rightarrow ^{212}\text{Bi}$	238	$84.9 \pm 3.7$	$71.3 \pm 2.4$	$81.7 \pm 3.4$
$^{228}\text{Ac} \rightarrow ^{228}\text{Th}$	338	$22.7 \pm 1.9$	$22.2 \pm 1.4$	$16.6 \pm 1.5$
$^{228}\text{Ac} \rightarrow ^{228}\text{Th}$	911	$21.8 \pm 1.9$	$18.8 \pm 1.3$	$17.8 \pm 1.6$
$^{137}\text{Cs} \rightarrow ^{137}\text{Ba}$	662	$6.8 \pm 1.0$	$6.6 \pm 0.7$	$5.0 \pm 0.8$
$^{60}\text{Co} \rightarrow ^{60}\text{Ni}$	1173	$0.5 \pm 0.3$	$1.7 \pm 0.4$	$2.2 \pm 0.6$
$^{60}\text{Co} \rightarrow ^{60}\text{Ni}$	1332	$1.7 \pm 0.5$	$1.4 \pm 0.3$	$2.2 \pm 0.6$
$^{40}\text{K} \rightarrow ^{40}\text{Ar}$	1461	$17.2 \pm 1.6$	$15.1 \pm 1.1$	$15.5 \pm 1.5$

Table 7: Comparison of results taken during nitrogen flushing at 1 l/min and 5 l/min. The area in grey are the radon daughter isotopes decays.



The results show a slight improvement to the 1 l/min flushing results. However, there also appears to be an increase in the previously reduced  $^{212}\text{Pb}$  peak. Given the  $^{228}\text{Ac}$  has

not increase, this could suggest contaminants were introduced into the detector volume which has a high thoron emanation.

### 8.3 Improvements to sensitivity

The reduction of the radon and its daughter isotopes translates to improved sensitivity for the  $^{238}\text{U}$  lines. This can be seen in Fig 24, where sensitivity is plotted as a function of time for the  $^{214}\text{Bi}$ , 609 keV, line.

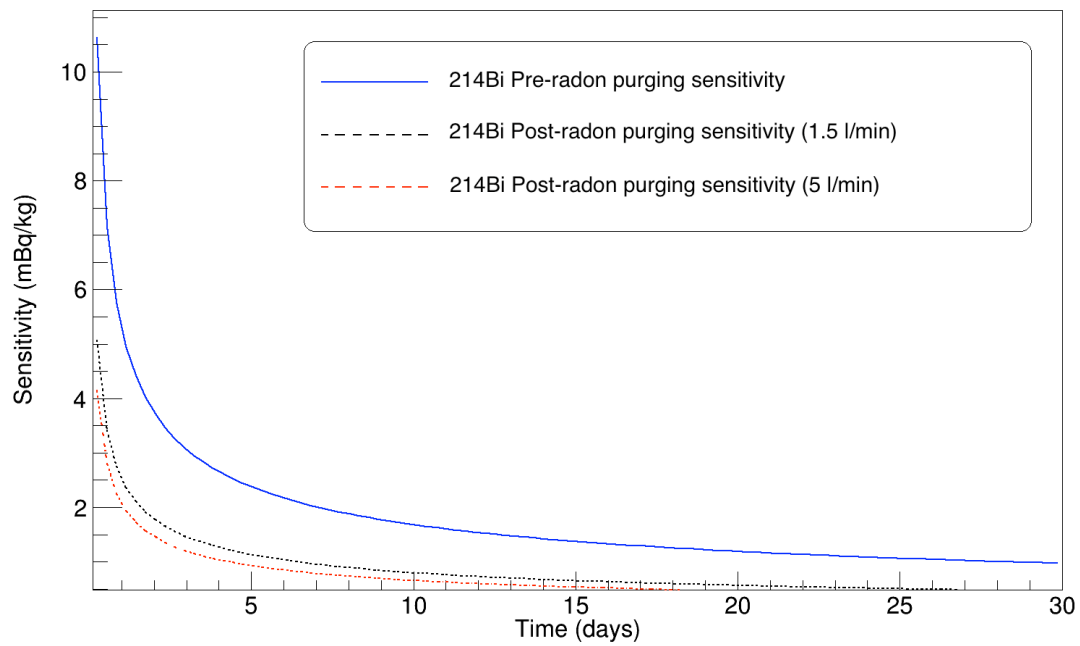


Figure 24: Sensitivity plot of the  $^{214}\text{Bi}$  line for no nitrogen flushing, 1 l/min and 5 l/min shown as blue, black and red respectively.

## 9 Discussion

Throughout the experiment, there has been several areas for future consideration and as well as room for possible improvements. Some of these are discussed here.

### 9.1 Detector improvements

There are current plans to expand the present lab and re-establish a designated low-background screening room. The current detector is located next to one side of the lab in close proximity of the wall, due to demands on space and convenience. The building materials contains small amounts of uranium, thorium and in particular potassium. Even with Pb and Cu shielding, it would be best to place the detector near the center of the room to minimise external gamma-rays.

To ensure absolute low background, radio-pure acid solutions should be used in the cleaning process of copper. Acid which enters into the pores of copper are difficult to remove, hence residual acid could contribute to contamination.

### 9.2 Further improvements to radon purging

To reduce the radon levels inside the detection volume, two of the three steps mentioned in Chapter 6 were taken. Since the MC simulation suggests further reductions are possible, the next step would be to introduce sealed containers filled with radon free gas into the central volume. This would reduce the volume which needed to be purged and the amount of nitrogen needed to flush it. The main difficulty is in finding containers made of radio-pure materials which can be filled and sealed securely.

Another improvement would be to use boil off nitrogen instead of cylindered nitrogen, as it is available in much greater abundance in the underground facility and contain far less radon contamination[11]. Cylindered nitrogen is currently used, as presently there is no way to control the flow rate of boil off nitrogen.

Boil off nitrogen also cannot be feed directly into the detector volume as it is too cold and generates condensation inside the sample volume. However, a long term solution could require the construction of a buffer volume which can be filled with boil off nitrogen which can then be feed into the detector volume.

### 9.3 External noise

During long background measurements at the present detector location, an increase in low energy noise was observed at certain time in the day. This was first attributed to the crane movement in the main laboratory which was then confirmed.

However, similar noise was also observed at times when no one was present inside the laboratory itself. After studying the times when the noise was present after several weeks, the source was found to be a laboratory inspector visiting each morning at 6 am and switching on the kettle.

## 9.4 RAD7

For the purposes of application, the humidity correction factors were studied over a short range. Given more time, a study over a greater range could be conducted as presently the humidity correction applied at the very low and high humidities are unknown. It is likely that the correction factor over a larger range will not be linear.

The intrinsic background measurement result could be improved by measuring over a longer period of time. Also long measurements of the laboratory using the DRYSTIK-ADS2 instead of the desiccant column should be made to get a more reliable value for the radon levels in the air.

There are several limitations with regard to the RAD7 detector and the CAPTURE software. Firstly, the same humidity correction factor is applied for both  $^{218}\text{Po}$  and  $^{214}\text{Po}$ . However, the  $^{214}\text{Po}$  should have a higher efficiency as when the neutralised  $^{218}\text{Po}$  decay, they will produce positive  $^{214}\text{Pb}$  ions that can be partly attracted to the detector. This process repeats until  $^{214}\text{Bi}$ , resulting in extra channels for the  $^{214}\text{Po}$  to reach the  $\alpha$  detector[12].

The CAPTURE software also does not take into account temperature effects on the counting efficiency which has been shown to be a contributing factor[13]. However, the detection efficiency variation as a result of temperature and humidity is difficult to independently model as there is a dependence on the volume of the detector and the drift length.




## 10 Conclusion

The objective of the project has been to demonstrate that the HPGe detector located at Boulby underground laboratory was fully operation and ready for material screening for the SuperNEMO experiment. This was done in three main parts;

- Calibrate the detector to allow **spectrums** taken by the germanium spectrometer to be analysed from which reliable measurements of the activity of a sample can be obtained.
- Modify and clean the detector shielding to eliminate direct line-of-sight gamma-rays to the detector and reduce internal contamination.
- Determine and minimise radon contributions to background measurement in order to improve detector sensitivity.

The detector was calibrate initially using point sources  $^{137}\text{Cs}$ ,  $^{60}\text{Co}$ ,  $^{57}\text{Co}$  and a Multi-Gamma source (MGS) containing in addition  $^{65}\text{Zn}$  and  $^{155}\text{Eu}$ . By plotting the known energy peaks of the sources with the mean of measured ADC peaks, a equation can be found to convert from ADC to energy. Then by fitting the peaks and measuring the variation of  $\sigma$  with energy, a resolution calibration was performed. Finally, by matching the MGS with known activities with data simulated using Geant4, an efficiency calibration was performed. This showed that the detector was ready to make reliable measurements.

Then the detector shielding was improved first by cleaning the Pb and Cu with alkaline and acidic solutions respectively to remove any surface residual. Then reconstructed to ensure uniform coverage of the detector, no direct line-of-sight gamma-rays to the detector and reproducibility as well as maintaining accessibility. This has been shown to reduce the integrated background counts between 100-2700 keV by approximately 20%.

The amount of radon present in the air of the laboratory was measured to be  $2.5 \pm 0.1$  Bq/m<sup>3</sup> using the RAD7. From this the radon contribution to the background was simulated using MC and showed significant improvements were possible by its removal. Hence a radon shield was constructed and a nitrogen flushing system was setup. Using both together showed a factor 4 improvement on the daughter decay peaks of  $^{222}\text{Rn}$ , and a  $\sim 30\%$  reduction again in the integrated rate between 100-2700 keV to  $0.751 \pm 0.001$ . Translating to improved sensitivity of the detector for the  $^{238}\text{U}$  lines 

Therefore, it can be concluded that the HPGe detector at Boulby underground laboratory is fully operational and capable of making reliable measurements of sample activity with competitive sensitivity. It is now ready for use in material screening and selection for the SuperNEMO experiment.

## 11 References

- [1] CERN, “Platform for the simulation of the passage of particles through matter using monte carlo methods,” <http://geant4.cern.ch>.
- [2] B. N. Laboratory, “National nuclear data center,” <http://www.nndc.bnl.gov/nudat2/>.
- [3] CERN, “An object oriented framework for large scale data analysis.,” <http://root.cern.ch/drupal/>, vol. Version 5.26.
- [4] U. dark matter collaboration, “UK DM project: radioactivity test results,” <http://hepwww.rl.ac.uk/ukdmc/Radioactivity/useful.html>.
- [5] J. P. Stewart and D. Groff, “Labsocs™ vs. source-based gamma-ray detector efficiency comparisons for nuclear power plant geometries,” *Paper presented at the 48th Annual Radiobioassay and Radiochemical Measurements Conference*, 2002.
- [6] L. Baudis and A. e. a. Ferella, “Gator: a low-background counting facility at the gran sasso underground laboratory,” *Journal of Instrumentation*, vol. 6, p. P08010, January 2012.
- [7] G. Heusser, M. Laubenstein, and H. Neder, “Low-level germanium gamma-ray spectrometry at the bq/kg level and future developments towards higher sensitivity,” in *Radionuclides in the Environment Int. Conf. On Isotopes in Env. Studies* (P. Povinec and J. Sanchez-Cabeza, eds.), vol. 8 of *Radioactivity in the Environment*, pp. 495 – 510, Elsevier, 2006.
- [8] D. radon instrumentation, *RAD7 RADON DETECTOR*. DURRIDGE Company, 524 Boston Road, Billerica, MA 01821, revision 7.2.2. ed., 2013.
- [9] DURRIDGE, “Rad7 communications software,” <http://www.durridge.com>.
- [10] DURRIDGE, “Drystik model ads-2,” <http://www.durridge.com>.
- [11] G. Gilmore, *Practical Gamma-ray Spectrometry*. Wiley, second edition ed., 2008.
- [12] J. Kiko, “Detector for  $^{222}\text{Rn}$  measurements in air at the 1 mbq/m<sup>3</sup> level,” *Nuclear Instruments and Methods in Physics Research A*, pp. 272–277, 2001.
- [13] V. Roca, P. De Felice, A. M. Esposito, C. Sabbarese, and J. Vaupotich, “The influence of environmental parameters in electrostatic cell radon monitor response,” *Applied Radiation and Isotopes*, vol. 61, pp. 243–247, August-September 2004.